

# Femtosecond laser induced periodic surface structures for the enhancement of field emission properties of tungsten

MAHREEN AKRAM,<sup>1,2\*</sup> SHAZIA BASHIR,<sup>1</sup> SOHAIL ABDUL JALIL<sup>3,4</sup>, MOHAMED ELKABBASH,<sup>3</sup> FRIEDRICH AUMAYR,<sup>2</sup> ALI AJAMI,<sup>2</sup> WOLFGANG HUSINSKY,<sup>2</sup> KHALIQ MAHMOOD,<sup>1</sup> MUHAMMAD SHAHID RAFIQUE<sup>5</sup> AND CHUNLEI GUO<sup>3,4\*</sup>

<sup>1</sup>Centre for Advanced Studies in Physics, Government College University, Near Secretariat Church Road, Lahore 54000, Pakistan

<sup>2</sup>Institute of Applied Physics, Vienna University of Technology, Vienna, Austria

<sup>3</sup>GPL, State Key Laboratory of Applied Optics, Changchun Institute of Optics, Fine Mechanics and Physics, Chinese Academy of Sciences, Changchun 130033, China

<sup>4</sup>The Institute of Optics, University of Rochester, Rochester, NY 14627, USA

<sup>5</sup>Department of Physics, University of Engineering and Technology, Lahore, Lahore 54000, Pakistan

\*[maharakram@gcu.edu.pk](mailto:maharakram@gcu.edu.pk) (Mahreen Akram) and \*[guo@optics.rochester.edu](mailto:guo@optics.rochester.edu) (Chunlei Guo)

**Abstract:** Direct femtosecond laser ablation enables the maskless fabrication of nano- and micro-scale structures on variety of materials. A typical example is the formation of femtosecond Laser Induced Periodic Surface Structures (fs-LIPSSs), which can lead to strong modification in electrical, optical, wetting, and field emission properties of materials. Here, we study the field emission properties of fs-LIPSSs. We created fs-LIPSSs and fs-LIPSSs covered with nano and micro-scale structures at different laser fluences on Tungsten (W) and showed that these structures offer significant enhancement in electron field emission properties. We provide a phenomenological model to explain the enhancement of electron emission parameters. The enhancement in the field emission properties of laser irradiated W is explained based on the convergence of electric field lines at the ridges of the fs-LIPSSs and fs-LIPSSs covered with nanoscale structures, which in turn, enhances the local field intensity and the electron emission parameters. The direct fabrication of 1D subwavelength structures is an important step towards the creation of low-cost cathodes for various potential applications.

© 2019 Optical Society of America under the terms of the [OSA Open Access Publishing Agreement](#)

## 1. Introduction

Subwavelength periodic surface structures were shown to modify the electrical, optical, mechanical and wetting properties of materials [1-4]. Ultrafast laser surface-processing can successfully produce different types of sub-wavelength structures such as cones, holes and fs-LIPSSs [1,2,5,6]. Among these structures, fs-LIPSSs have been extensively studied as they offer a facile way of achieving a well-organized and highly precise patterns [7-9]. The underlying mechanism of fs-LIPSSs is not fully understood and widely discussed in the literature [7-9], however, on metals, it is commonly believed to be a result of interference between the incident light and the scattered surface waves, namely, surface plasmons polaritons (SPPs) [1,10]. Briefly, the irradiation of a smooth surface create surface roughness with multiple femtosecond laser pulses and excite SPPs that interferes with the incident radiation resulting in a spatial distribution of the field intensity across the material surface which leads to selective, periodic ablation [1,11]. Fs-LIPSSs have been employed for wide range of applications such as structural colorization, perfect light absorption, anti-reflective surfaces and improved wetting properties [1,12-14].

On the other hand, electron sources with high stability and enhanced efficiency are desirable for various applications such as flat panel displays and field emission electron microscopes [15,16]. Periodic arrays of microtips are commonly used as large area field emission (FE) cathode in integrated circuits, flat-panel displays and microwave power amplifiers [15,17]. The development of such cathodes operating at low voltages with high current density is significantly important and reported by many research groups [18-21]. Large area regular arrays of FE tips were fabricated using electron beam lithography, electrodeposition, hydrothermal or electrochemical techniques [18-20,22]. Although, the emission from such high aspect-ratio cathodes is highly directional [23-25], these methods are complex and expensive. On the other hand, laser induced surface structuring as a result of direct laser ablation is a potential alternative for the fabrication of large area FE cathodes. This method exhibits simplicity, robustness and ease of fabrication. Recently, enhancement in the FE properties have been reported for the nanosecond and femtosecond laser irradiated structures [26-31]. In addition, we reported the surface-plasmon-enhanced

photoelectron emission from nanostructure-covered periodic grooves on metals [32]. Nevertheless, the FE enhancement from fs-LIPSSs formed on metallic surfaces has not been reported previously.

Here, we study the enhancement of field emission properties from the fs-LIPSSs and fs-LIPSSs covered with nano- and micro-scale structures. All type of Fs-LIPSSs structures show a significantly higher enhancement in the electron emission parameters. We show that fs-LIPSSs enhanced FE properties depend on laser fluence  $F$ . We provide a phenomenological model to explain the enhancement of electron emission parameters. Our model employs the convergence of electric field at the ridges of the fs-LIPSSs, which in turn, enhance the electron emission parameters.

## 2. Experimental setup

A diagram of the experimental setup is illustrated in Fig. 1, where a Ti: sapphire femtosecond laser amplifier (Femtopower Compact Pro, Femtolasers productions GmbH, Austria) was employed as an irradiation source to deliver horizontally polarized pulse trains at the repetition rate of 1 kHz, with central wavelength of  $\lambda=800$  nm and a pulse duration of  $\tau=30$  fs.

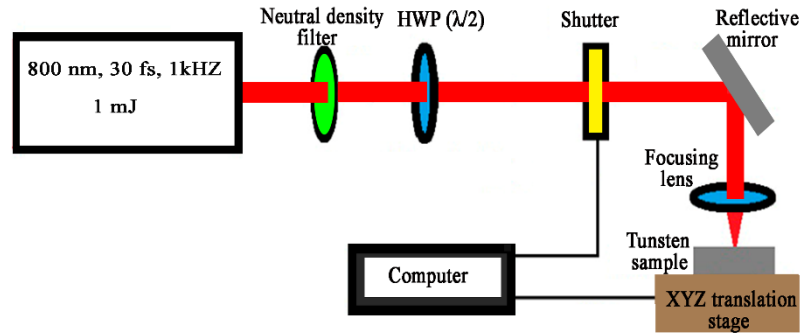


Fig. 1. A schematic of the experimental setup for the formation of subwavelength structures on the tungsten surface, using femtosecond laser beam.

The maximum pulse energy delivered by the laser system is 1 mJ, which was attenuated with the help of neutral density filters. A half wave-plate ( $\lambda/2$ ) was employed to change the light polarization from horizontal to vertical direction. An electromechanical shutter was used to select a single shot for controlling the number of shots. The laser was focused by a lens of focal length 10 cm and incident at normal incidence. A bulk circular disk of W (obtained from Alfa Aesar company with 99.95% purity) of diameter 20 mm and thickness 5 mm was used as a target material due to its high electronic emissivity, superior thermal and chemical stability and excellent mechanical strength [33,34]. The sample was mounted at a computerized XYZ precision stage and translated at a fixed speed of 1 mm/s for all experiments, which give 99.2 percent overlap between pulses. In order to avoid overlap of scanned lines, the step size or interspacing between two lines is kept constant of 100  $\mu\text{m}$ . Accordingly, the scanned lines are formed throughout the surface. The laser fluence was varied by increasing the power. After the laser microstructuring process, the surface morphology was analyzed by Scanning Electron Microscopy (SEM) and electron emission performance was investigated through field emission measurements. The experimental setup for field emission measurements is shown elsewhere [31].

## 3. Results and Discussions

To determine the effect of surface structuring for the enhancement of FE properties, we first investigate the formation of fs-LIPSSs at various laser fluences. The overall scanned pattern of the laser irradiated region is shown in the Fig. 2(a). The optimal results suitable for FE enhancement are presented in Fig. 2(b-e) and were obtained using laser fluences of (b) 0.09 J/cm<sup>2</sup>, (c) 0.18 J/cm<sup>2</sup>, (d) 0.90 J/cm<sup>2</sup>, and (e) 1.81 J/cm<sup>2</sup>. As shown in Fig. 2(b), a well-defined fs-LIPSSs structures observed with periodicity of  $\Lambda \sim (634 \pm 0.48)$  nm. Accordingly, low-spatial-frequency LIPSSs (LSFLs) are created with spatial orientation perpendicular to the incident laser polarization (vertically polarized) as reported by others [35,36]. Closer inspection of Fig 2(b) reveal that such surface structures have a slanted distribution of ridges and grooves, i.e., elongated grooves and ridges in the range of 10<sup>3</sup>'s of microns. The observed slanted behavior of fs-LIPSSs is due to random scattering that acts as a seed points for fs-LIPSSs [7]. We note here the decrease in fs-LIPSSs period to  $(590 \pm 0.88)$  by increasing the fluence to 0.18 J/cm<sup>2</sup> (Fig. 2c). In addition, the ridge width is reduced, and grooves become more pronounced. By further increasing the fluence to

0.90 J/cm<sup>2</sup>, the scanned line region in Fig. (2d) shows enhanced nanoscale particulates at the grooves and ridges of fs-LIPSSs which make them diffusive. The measured fs-LIPSSs groove periodicity of (602 ± 0.88) nm is observed across the ablated region, which is considerably smaller than the period obtained with the lowest fluence of (0.09 J/cm<sup>2</sup>). We also note that at the fluence of ( $F = 0.9$  J/cm<sup>2</sup>), extensive nanoscale structures are formed that are randomly distributed (Fig. 2d). For the highest fluence ( $F = 1.81$  J/cm<sup>2</sup>), nano- and micro-scale structures are formed and the overall LSFLs morphology is distorted due to increased melting and re-solidification (Fig. 2e). Craters formation can be seen along with microscale structures. Figure 2(f) shows two-dimensional Fast Fourier transform (2D-FFT) of the fs-LIPSS obtained at the fluence of 0.09 J/cm<sup>2</sup> which reflects its uniformity. We note that the fs-LIPSSs periodicity for fluences ( $F = 0.09, 0.18$  and  $0.9$  J/cm<sup>2</sup>), were obtained using the 2D-FFT analysis.

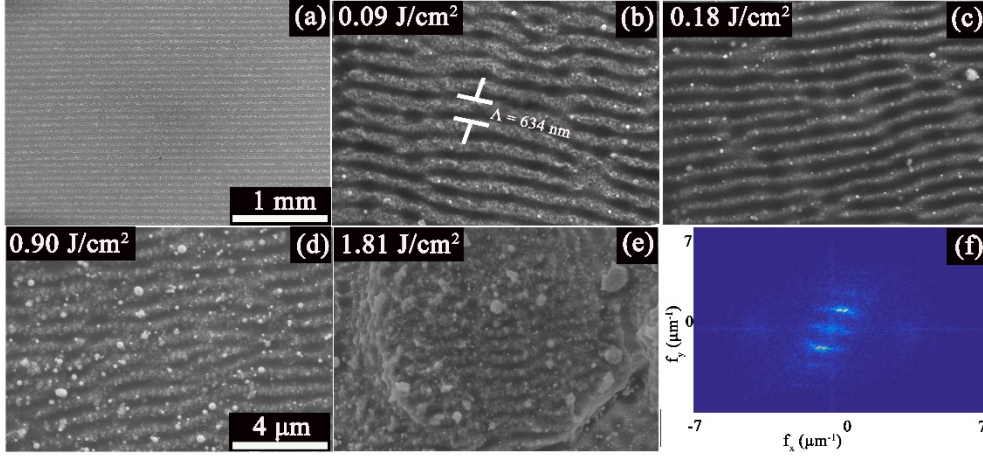


Fig. 2. (a) An image of entire scanned region shown for the overall scanned target at the fluence of **1.81 J/cm<sup>2</sup>**. SEM image of 1D uniform fs-LIPSSs by irradiation of single beam femtosecond laser pulses at the fluence of (b) **0.09 J/cm<sup>2</sup>** (c) fs-LIPSSs with nanostructures **0.18 J/cm<sup>2</sup>** and (d) fs-LIPSSs with nano- and micro-scale structures formed at the fluences of **0.90 J/cm<sup>2</sup>** and **1.81 J/cm<sup>2</sup>**. (e) Extensive nano- and micro-scale structures formed at the ridges and grooves of the fs-LIPSSs at the fluence of **1.81 J/cm<sup>2</sup>**. The scale-bar of 4μm is same for Fig. 2(b-e). (f) An image of fast fourier transform of the fs-LIPSSs structures in Fig. 2(b).

The formation of fs-LIPSSs has been extensively investigated by us and others [11,37,38]. Briefly, the irradiation of a smooth surface with multiple fs laser pulses excite surface waves SPPs that interferes with the incident radiation resulting in a spatial distribution of the field intensity across the material surface which leads to selective, periodic ablation. The formed grooves, thus, have a wave-vector  $\mathbf{G}$  such that  $\mathbf{G} = \mathbf{k}_i - \mathbf{k}_{SPP}$ , where  $\mathbf{k}_i = 2\pi|\lambda_i|^{-1}$  and  $\mathbf{k}_{SPP} = 2\pi|\lambda_{SPP}|^{-1}$  are the incident laser beam and the SPP wave-vectors, respectively and  $\lambda_i$  and  $\lambda_{SPP}$  are the incident laser wavelength and SPP wavelength, respectively. For an incident angle  $\theta$  (measured from the normal),  $\mathbf{G} = \mathbf{k}_i \sin \theta - \mathbf{k}_{SPP}$ , since only the wavevector component parallel to the metal-dielectric interface excites SPPs. The grooves' period is given by  $\Lambda = 2\pi/|\mathbf{G}| = 2\pi/|(\frac{2\pi \sin \theta}{\lambda_i} - \frac{2\pi}{\lambda_{SPP}})|$ . Consequently  $\Lambda = \lambda_i / |\sin \theta - \frac{\lambda_i}{\lambda_{SPP}}|$ , and finally, we obtain the period  $\Lambda$  of near subwavelength fs-LIPSSs as below [38];

$$\Lambda = \frac{\lambda_i}{\frac{\lambda_i}{\lambda_{SPP}} \pm \sin \theta} \quad (1)$$

For normal incidence (when  $(\theta = 0^\circ)$ , as in our case,  $\Lambda = \lambda_{SPP}$ . Thus, the period of fs-LIPSSs is  $\lambda_{SPP}$ . For a metal its complex permittivity is given by  $\tilde{\epsilon} = \epsilon_m^{Re} + i\epsilon_m^{Im}$ , where,  $\epsilon_m^{Re}$  and  $\epsilon_m^{Im}$  are the real and imaginary parts of the metal permittivity. The excitation of a surface wave at a metal-dielectric interface, thus, requires a phase mismatch with the dielectric, i.e., the guided mode is to the right of the light-line,  $\lambda_{SPP}$  is highly sensitive to the metal and dielectric permittivity [38],  $\lambda_{SPP} = \lambda_i \left( \frac{\epsilon_m^{Re} + \epsilon_D}{\epsilon_m^{Re} \epsilon_D} \right)^{1/2}$ , where  $\epsilon_D$  is the dielectric permittivity and  $\epsilon_m^{Re}$  is the real part of the metal's complex permittivity [38,39]. In other words, at fluence higher than damage threshold, the fs-LIPSSs formed on the material will be equal to  $\lambda_{SPP}$ , which is always smaller than the incident wavelength as we observed.

Although W is not a metal at the excitation wavelength of 800nm ( $\epsilon_m^{Re}(800nm) = 5.22$ ), the excitation of SPP is still possible due to the high intensity associated with fs laser pulses which promotes enough electrons beyond the W bandgap such that it transiently behaves as a metal, i.e.,  $\epsilon_m^{Re} < -1$  [39]. Furthermore, the reduced  $\Lambda$  for fluences

$F = (0.18 \text{ and } 0.9 \text{ J/cm}^2, \text{ compared to } 0.09 \text{ J/cm}^2)$ , is due to increase in the effective dielectric permittivity as surface roughness formed on the W surface, which leads to the reduction in  $\lambda_{\text{SPP}}$  [37,40].

### 3.1. Field Emission analysis

The electron emission performance such as turn-on field, field enhancement factor and current density of fs-LIPSSs and fs-LIPSSs covered micro and nanoscale structures with respect to untreated target are analyzed using the Fowler–Nordheim (FN) equation based on the FE theory proposed for metallic electron emitters [41]. It relates the emitted  $J$  to the applied field ( $E$ ) at the metallic emitter surface as follows;

$$J = a(E^2 \beta^2 \varphi) \exp\left(\frac{-b\varphi^{3/2}}{\beta E}\right) \quad (2)$$

where  $a$  and  $b$  are constants whose values are listed as  $1.4 \times 10^{-6}$  and  $-6.83 \times 10^9$ , respectively. Since  $E = \frac{V}{d}$ , where, “ $E$ ,  $V$  and  $d$ ” are the applied electric field, voltage and inter-electrode spacing, respectively. In our experiments, we varied the voltage ranging from 0.1 kV to 2.5 kV and kept the inter-electrode spacing to  $d = 200 \mu\text{m}$ . The current density is generally defined as,  $J = \frac{I}{A}$ , where,  $A$  is area of electrode, that is  $15 \text{ mm}^2$ , and  $\varphi$  is a work function. As we have irradiated the samples in ambient air and presence of oxides peak is evident from the XRD analysis, hence, we have used work function of tungsten oxide (5.7 eV) for the field emission analysis. An important factor in field emission is the relationship between the applied and the local electric field where electron tunneling occurs [31,41,42]. For this tunneling, the field enhancement factor ( $\beta$ ) is defined by;  $\beta = \frac{E_{\text{loc}}}{E_{\text{app}}}$ , where  $E_{\text{loc}}$  is the local field enhancement and  $E_{\text{app}}$  is the applied electric field, plays a key role.

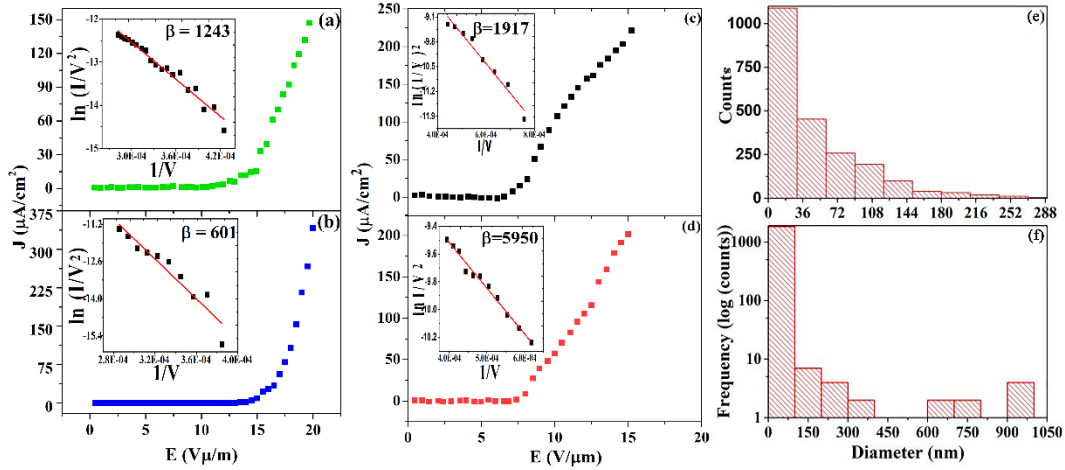


Fig. 3. J-E plots of the laser irradiated W at the fluences of (a) 0.09 J/cm<sup>2</sup>(b) 0.18 J/cm<sup>2</sup>, (c) 0.90 J/cm<sup>2</sup>and (d) 1.81 J/cm<sup>2</sup>. The corresponding FN plots are shown in the insets. (e-f) The diameter of nano- and microscale structures measured from SEM images, formed at the fluences of 0.90 J/cm<sup>2</sup> and 1.81 J/cm<sup>2</sup>, respectively.

Equation (2), can be written in terms of  $I$  and  $V$  and inserting the values of constants “ $a$ ” and “ $b$ ”, we obtain;

$$I = (1.4 \times 10^{-6}) \left( \frac{A\beta^2 V^2}{d^2 \varphi} \right) \exp\left(-6.83 \times 10^9 \frac{\varphi^{3/2} d}{\beta V}\right) \quad (3)$$

The value of  $\beta$  can be extracted from the linear slope ( $m$ ) of the plot between  $\ln(I/V^2)$  versus  $1/V$  as follows;

$$\beta = -6.83 \times 10^9 \left( \frac{\varphi^{3/2} d}{m} \right) \quad (4)$$

Figures 3 (a–d) illustrate  $J$  versus  $E$  plots along with the corresponding FN plots in insets for the laser irradiated W samples at different fluences of (a) 0.09 J/cm<sup>2</sup>(b) 0.18 J/cm<sup>2</sup>, (c) 0.90 J/cm<sup>2</sup>and (d) 1.81 J/cm<sup>2</sup>. The current density essentially remains zero until turn-on field, which in our case, we defined as the applied electric field require to attain a current density of  $\sim 10 \mu\text{A/cm}^2$  and the current exponentially increases afterwards. From Fig. 3(a-d), the linear nature of the FN plots with a single negative slope and minimum deviation from linearity ensures the field emission as the origin of the measured current. The maximum applied voltage and hence the field is limited to pre-

breakdown regime and before saturation. The obtained FE parameters for samples irradiated at different fluences are summarized in the Table 1.

**Table 1. Obtained field emission parameters for irradiated W samples at different fluences.**

Fluence ( $\text{J}/\text{cm}^2$ )	$E_0$ ( $\text{V}/\mu\text{m}$ )	$\beta$	$J$ ( $\mu\text{A}/\text{cm}^2$ )
0.09	13.5	1243	146 @ $E = 20 \text{ V}/\mu\text{m}$
0.18	15	601	341 @ $E = 20 \text{ V}/\mu\text{m}$
0.90	7	1917	217 @ $E = 16 \text{ V}/\mu\text{m}$
1.81	8	5950	200 @ $E = 16 \text{ V}/\mu\text{m}$

For the fluence of  $0.09 \text{ J}/\text{cm}^2$ , the turn-on field of  $13.5 \text{ V}/\mu\text{m}$ ,  $\beta = 1243$  and  $J = 146 \mu\text{A}/\text{cm}^2$  at  $E = 20 \text{ V}/\mu\text{m}$ . Enhancement in field emission parameters has been reported for microscale and nanoscale structures with high aspect ratio such as nanorods, nanowires, nanostructures and conical structures [24,25,43]. The applied electric field significantly localizes at the apex of these structures and locally enhances the electric field [41]. On the other hand, a planar diode configuration would require several kilovolts to realize cold emission in the absence of surface structure induced field localization [23]. In the case of fs-LIPSSs, the formed surface structures enable the localization of the applied electric field which enhances the field emission parameters. In particular, fs-LIPSSs consisting of ridges (protuberance) and grooves (valley region) with a ridge-to-valley depth in the order of  $\sim 150 \text{ nm}$  [44] such that the electric field is localized at the fs-LIPSSs ridges as schematically shown in Figure 4.

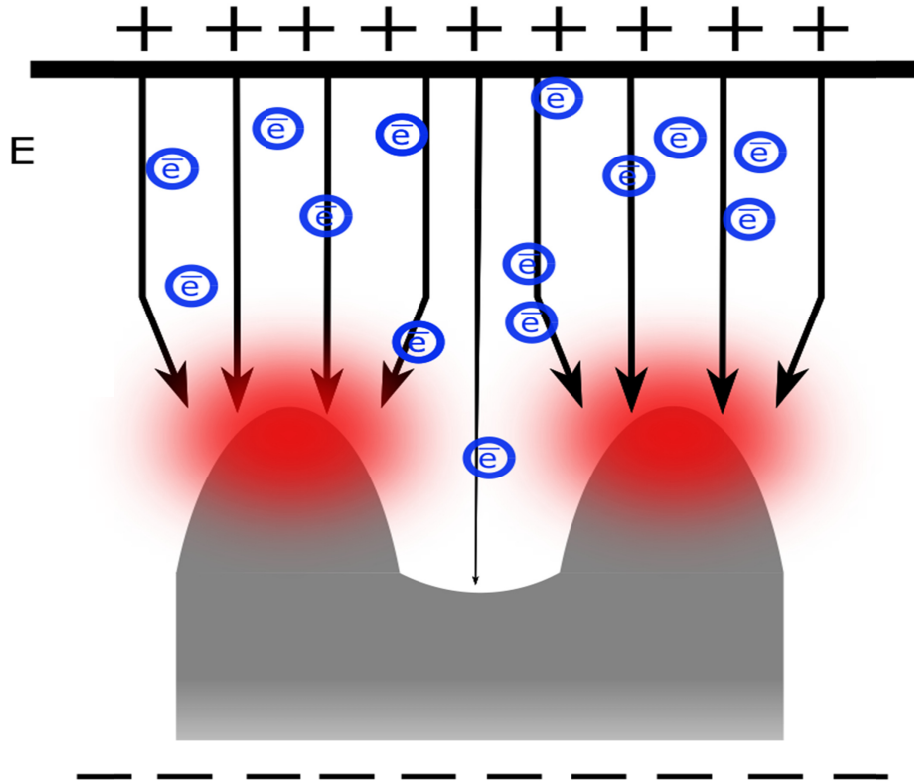


Fig. 4. Physical mechanism involved in electron emission from fs-LIPSSs on the tungsten surface in response to the applied electric field. Cross-sectional area of fs-LIPSSs structures containing grooves and ridges, favorable for the convergence of applied electric field. The arrows denote the maximum field at the ridges of fs-LIPSSs due to difference in peak-to-valley region.

By increasing the fluence up to  $0.18 \text{ J}/\text{cm}^2$ , fs-LIPSSs morphology with reduced ridge width ( $280 \pm 40$ ) nm is observed as compared to ( $530 \pm 40$ ) nm at  $0.09 \text{ J}/\text{cm}^2$ , and increased groove width from ( $280 \pm 40$ ) nm to ( $390 \pm 60$ ) nm exhibits a decrease in the value of  $\beta$  to 601 and increase in the turn-on field to  $15 \text{ V}/\mu\text{m}$  and maximum current density to a value of  $341 \mu\text{A}/\text{cm}^2$ . The reduction in the ridge width in parallel with the decrease in the  $\beta$

value supports our proposed model for the enhancement of field emission properties due to the convergence of field lines at the ridges. Lesser the ridge width corresponds to more area occupied by grooves, as we quantitatively shown above, hence less will be the value of  $\beta$ . The significant increase in the current density with a decreased  $\beta$  suggests either an increase in the emission area or decrease in the work function [45]. This can also be explained on the basis of reduced screening effect as it is reported that emission current increases with the increase of spacing (in our case the groove width) between the emitter up to a certain value [46]. For the sample irradiated at  $0.90 \text{ J/cm}^2$ , a low turn-on field of  $7 \text{ V}/\mu\text{m}$ , and a high beta factor of value 1917 is achieved along with a maximum current density of  $217 \mu\text{A}/\text{cm}^2$ , at  $16 \text{ V}/\mu\text{m}$ . This is attributed to the nanostructures covered fs-LIPSSs morphology. Such nanostructures have been shown for the enhancement of field emission due to increased surface area [47]. For W irradiated with maximum fluence, a significant increase in the value of  $\beta=5950$  is observed as depicted in Fig. 3(d). However, the turn-on field slightly increased to  $8 \text{ V}/\mu\text{m}$  whereas, maximum current density decreases to  $200 \mu\text{A}/\text{cm}^2$ .

Quantitatively, for the highest fluence of  $F = 1.81 \text{ J/cm}^2$ , the density of nanoscale structures (Fig. 3 (f)) is lower than what we obtained for the fluence of  $F = 0.90 \text{ J/cm}^2$  (Fig. 3(e)). Accordingly, the increase in the size of the nanostructures that cover the fs-LIPSSs correspond to an increased value of  $\beta$ . The increase in the turn-on and decrease of the maximum current density for the highest fluence is explained based on screening effect [46].

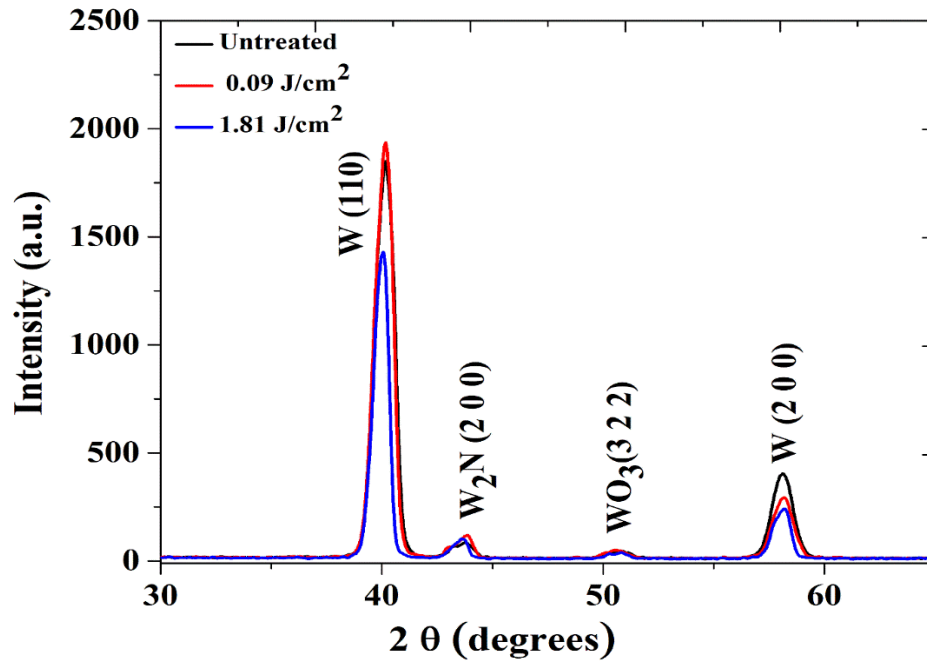


Fig. 5. XRD patterns of the untreated and laser irradiated W at the fluence of  $0.09 \text{ J/cm}^2$  and (b)  $1.81 \text{ J/cm}^2$ .

Figure 5 shows the XRD results of the structural and compositional phases of untreated and laser irradiated W targets at low and high fluence of  $0.09 \text{ J/cm}^2$  and  $1.81 \text{ J/cm}^2$ . The XRD analysis shows that all samples have the peaks corresponding to W,  $\text{W}_2\text{N}$  and  $\text{WO}_3$  phases. The peaks at  $2\theta$  values of  $40.265^\circ$  and  $58.276^\circ$  correspond to W (1 1 0) and W (2 0 0) orientations and are attributed to the JCPD reference pattern (00-004-0806). The peak at an angle of  $43.849^\circ$  is representing  $\text{W}_2\text{N}$  (2 0 0) phase and is attributed to the JCPD reference pattern (00-025-1257). The remaining small peak at  $50.886^\circ$  corresponds to the  $\text{WO}_3$  (3 2 2) phase and is indexed on the basis of JCPD reference pattern (00-020-1323). However, the W target irradiated at high fluence shows more pronounced peak shifting and decrease in intensities as compared to W target irradiated at low fluence. The reduction in both W (110) and W (200) is due to the loss of crystallinity, due to the fs laser surface ablation.

#### 4. Conclusions

We have successfully employed femtosecond laser irradiation to create periodic surface structures on the bulk tungsten surface. It is surprisingly found that these fs-LIPSSs structures show tremendous enhancement in electron field emission parameters. We show that fs-LIPSSs enhanced FE properties depends on laser fluence  $F$ . We provide

a plausible explanation for the formation of fs-LIPSSs and enhancement of field emission from these bare fs-LIPSSs and fs-LIPSSs covered with nano- and micro-scale structures. The direct fabrication of structured cathode opens an important step for future investigations for low-cost cathodes for various potential applications.

### Funding

This work is financially supported by the Bill & Melinda Gates Foundation (OPP1119542). Mahreen Akram acknowledges Higher Education Commission of Pakistan, for financial support to travel Vienna through IRSIP program.

### References

1. A. Y. Vorobyev and C. Guo, "Direct femtosecond laser surface nano/microstructuring and its applications", *Laser. Photonics Rev.* **7**(3), 385-407 (2013).
2. J. Bonse, S. Höhm, S. V. Kirner, A. Rosenfeld, and J. Krüger, "Laser-induced periodic surface structures—a scientific evergreen", *IEEE J. Sel. Top. Quantum Electron* **23**(3), 109-123 (2017).
3. K. Sugioka and Y. Cheng, "Ultrafast lasers—reliable tools for advanced materials processing", *Light. Sci. Appl.* **3**(4), e149 (2014).
4. M. Malinauskas, M. Farsari, A. Piskarskas, and S. Juodkazis, "Ultrafast laser nanostructuring of photopolymers: A decade of advances", *Phys. Rep.* **533**(1), 1-31 (2013).
5. J. Cheng, C.-s. Liu, S. Shang, D. Liu, W. Perrie, G. Dearden, and K. Watkins, "A review of ultrafast laser materials micromachining", *Opt Laser Technol* **46**(88-102) (2013).
6. R. Buividas, M. Mikutis, and S. Juodkazis, "Surface and bulk structuring of materials by ripples with long and short laser pulses: Recent advances", *Prog Quant Electron* **38**(3), 119-156 (2014).
7. B. Öktem, I. Pavlov, S. Ilday, H. Kalaycıoğlu, A. Rybak, S. Yavaş, M. Erdoğan, and F. Ö. Ilday, "Nonlinear laser lithography for indefinitely large-area nanostructuring with femtosecond pulses", *Nat. Photonics* **7**(11), 897 (2013).
8. S. A. Jalil, J. Yang, M. Elkabbash, S. C. Singh, and C. Guo, "Maskless formation of uniform subwavelength periodic surface structures by double temporally-delayed femtosecond laser beams", *Appl. Surf. Sci.* **471**(516-520) (2019).
9. G. D. Tsididis, M. Barberoglou, P. A. Loukakos, E. Stratakis, and C. Fotakis, "Dynamics of ripple formation on silicon surfaces by ultrashort laser pulses in subablation conditions", *Phys. Rev. B* **86**(11), 115316 (2012).
10. J. Bonse, A. Rosenfeld, and J. Krüger, "On the role of surface plasmon polaritons in the formation of laser-induced periodic surface structures upon irradiation of silicon by femtosecond-laser pulses", *J. Appl. Phys.* **106**(10), 104910 (2009).
11. J. Sipe, J. F. Young, J. Preston, and H. Van Driel, "Laser-induced periodic surface structure. I. Theory", *Phys. Rev. B* **27**(2), 1141 (1983).
12. A. Y. Vorobyev and C. Guo, "Colorizing metals with femtosecond laser pulses", *Appl. Phys. Lett.* **92**(4), 041914 (2008).
13. A. Vorobyev and C. Guo, "Metal pumps liquid uphill", *Appl. Phys. Lett.* **94**(22), 224102 (2009).
14. A. Y. Vorobyev, V. Makin, and C. Guo, "Brighter light sources from black metal: significant increase in emission efficiency of incandescent light sources", *Phys. rev. Lett.* **102**(23), 234301 (2009).
15. Q. Wang, A. Setlur, J. Lauerhaas, J. Dai, E. Seelig, and R. Chang, "A nanotube-based field-emission flat panel display", *Appl. Phys. Lett.* **72**(22), 2912-2913 (1998).
16. J. I. Goldstein, D. E. Newbury, J. R. Michael, N. W. Ritchie, J. H. J. Scott, and D. C. Joy, *Scanning electron microscopy and X-ray microanalysis* (Springer, 2017).
17. A. Karabutov, V. Frolov, E. Loubnin, A. Simakin, and G. Shafeev, "Low-threshold field electron emission of Si micro-tip arrays produced by laser ablation", *Appl. Phys. A* **76**(3), 413-416 (2003).
18. T. Hang, H. Ling, A. Hu, and M. Li, "Growth mechanism and field emission properties of nickel nanocones array fabricated by one-step electrodeposition", *J. Electrochem. Soc.* **157**(12), D624-D627 (2010).
19. X. LeQuan, B. Choi, W. Kang, and J. Davidson, "Nanodiamod lateral device field emission diode fabricated by electron beam lithography", *Diam. Relat. Mater.* **19**(2-3), 252-255 (2010).
20. J. Wang, L. Wei, L. Zhang, J. Zhang, H. Wei, C. Jiang, and Y. Zhang, "Controlled growth of nickel nanocrystal arrays and their field electron emission performance enhancement via removing adsorbed gas molecules", *CrystEngComm* **15**(7), 1296-1306 (2013).
21. E. Stratakis, R. Giorgi, M. Barberoglou, T. Dikonimos, E. Salernitano, N. Lisi, and E. Kymakis, "Three-dimensional carbon nanowall field emission arrays", *Appl. Phys. Lett.* **96**(4), 043110 (2010).

22. H. Yan, C. F. Blanford, B. T. Holland, M. Parent, W. H. Smyrl, and A. Stein, "A chemical synthesis of periodic macroporous NiO and metallic Ni", *Adv. Mater.* **11**(12), 1003-1006 (1999).
23. V. Zhirnov, C. Lizzul-Rinne, G. Wojak, R. Sanwald, and J. Hren, "Standardization" of field emission measurements", *J Vac Sci Technol B Microelectron Nanometer Struct Process Meas Phenom* **19**(1), 87-93 (2001).
24. C. Lee, T. Lee, S. Lyu, Y. Zhang, H. Ruh, and H. Lee, "Field emission from well-aligned zinc oxide nanowires grown at low temperature", *Appl. Phys. Lett.* **81**(19), 3648-3650 (2002).
25. R.-S. Chen, Y.-S. Huang, Y.-M. Liang, C.-S. Hsieh, D.-S. Tsai, and K.-K. Tiong, "Field emission from vertically aligned conductive IrO<sub>2</sub> nanorods", *Appl. Phys. Lett.* **84**(9), 1552-1554 (2004).
26. V. Zorba, I. Alexandrou, I. Zergioti, A. Manousaki, C. Ducati, A. Neumeister, C. Fotakis, and G. Amaratunga, "Laser microstructuring of Si surfaces for low-threshold field-electron emission", *Thin Solid Films* **453**(492-495) (2004).
27. D. J. Late, V. R. Singh, S. Sinha, M. A. More, K. Dasgupta, and D. S. Joag, "Synthesis of LaB<sub>6</sub> micro/nano structures using picosecond (Nd: YAG) laser and its field emission investigations", *Appl. Phys. A* **97**(4), 905 (2009).
28. A. Singh, D. Shinde, M. A. More, and S. Sinha, "Enhanced field emission from nanosecond laser based surface micro-structured stainless steel", *Appl. Surf. Sci.* **357**(1313-1318) (2015).
29. S. Jalil, S. Bashir, M. Akram, Q. Ahmed, and F. Haq, "Surface morphology correlated with field emission properties of laser irradiated nickel", *Indian. J. Phys.* **91**(8), 953-965 (2017).
30. A. Singh, S. R. Suryawanshi, M. More, S. Basu, and S. Sinha, "Field emission study from an array of hierarchical micro protrusions on stainless steel surface generated by femtosecond pulsed laser irradiation", *Appl. Surf. Sci.* **396**(1310-1316) (2017).
31. M. Akram, S. Bashir, S. A. Jalil, M. S. Rafique, A. Hayat, and K. Mahmood, "Investigation of field emission properties of laser irradiated tungsten", *Appl. Phys. A* **124**(2), 180 (2018).
32. T. Y. Hwang, A. Vorobyev, and C. Guo, "Surface-plasmon-enhanced photoelectron emission from nanostructure-covered periodic grooves on metals", *Phys. Rev. B* **79**(8), 085425 (2009).
33. Y.-H. Lee, C.-H. Choi, Y.-T. Jang, E.-K. Kim, B.-K. Ju, N.-K. Min, and J.-H. Ahn, "Tungsten nanowires and their field electron emission properties", *Appl. Phys. Lett.* **81**(4), 745-747 (2002).
34. K. Sun, J. Y. Lee, B. Li, W. Liu, C. Miao, Y.-H. Xie, X. Wei, and T. P. Russell, "Fabrication and field emission study of atomically sharp high-density tungsten nanotip arrays," (AIP, 2010).
35. J. Sipe, J. F. Young, J. Preston, and H. Van Driel, "Laser-induced periodic surface structure. I. Theory", *Physical Review B* **27**(2), 1141 (1983).
36. J. F. Young, J. Preston, H. Van Driel, and J. Sipe, "Laser-induced periodic surface structure. II. Experiments on Ge, Si, Al, and brass", *Phys. Rev. B* **27**(2), 1155 (1983).
37. A. Vorobyev, V. Makin, and C. Guo, "Periodic ordering of random surface nanostructures induced by femtosecond laser pulses on metals", *J. Appl. Phys.* **101**(3), 034903 (2007).
38. M. Huang, F. Zhao, Y. Cheng, N. Xu, and Z. Xu, "Origin of laser-induced near-subwavelength ripples: interference between surface plasmons and incident laser", *Acs nano* **3**(12), 4062-4070 (2009).
39. A. Vorobyev and C. Guo, "Femtosecond laser-induced periodic surface structure formation on tungsten", *J. Appl. Phys.* **104**(6), 063523 (2008).
40. E. Kröger and E. Kretschmann, "Surface plasmon and polariton dispersion at rough boundaries", *Phys. Status Solidi B* **76**(2), 515-523 (1976).
41. R. Fowler and L. Nordheim, "Field emission from metallic surfaces", *Proc. R. Soc. London. Ser. A* **119**(173-181) (1928).
42. D. Lu, A. Ogino, B. Liang, J. Liu, and M. Nagatsu, "Field-emission properties of nanostructured WO<sub>3</sub> arrays fabricated using tungsten hot-filament chemical vapor deposition", *Jpn. J. Appl. Phys.* **48**(9R), 090206 (2009).
43. H. Kosmahl, "Analytic evaluation of field emission enhancement factors for ellipsoidal cones and elliptic cross-section wedges", *IEEE Trans. Electron Devices* **38**(6), 1534-1537 (1991).
44. S. A. Jalil, J. Yang, M. ElKabbash, Y. Lei, W. He, and C. Guo, "Formation of uniform two-dimensional subwavelength structures by delayed Triple femtosecond laser pulse irradiation", *Opt. Lett.* **to be published**.
45. S. Kajita, N. Ohno, Y. Hirahata, and M. Hiramatsu, "Field emission property of nanostructured tungsten formed by helium plasma irradiation", *Fusion. Eng. design* **88**(11), 2842-2847 (2013).
46. G. Chen, W. Wang, J. Peng, C. He, S. Deng, N. Xu, and Z. Li, "Screening effects on field emission from arrays of (5, 5) carbon nanotubes: quantum mechanical simulations", *Phys. Rev. B* **76**(19), 195412 (2007).
47. M. Trapatseli, D. Vernardou, P. Tzanetakis, and E. Spanakis, "Field emission properties of low-temperature, hydrothermally grown tungsten oxide", *ACS Appl. Mater. Interfaces* **3**(7), 2726-2731 (2011).

